J-COSMICについてはPETに比してより汎用性の高い脳血流SPECTの研究であることから，研究成果をより広い範囲で活用することが可能である。また，画像を中心として多数例のMCIを対象とした前向きコホート研究を実施するうえでのノウハウは，その後の研究を実施するうえで貴重な財産となっている。J-COSMICとSEAD-Japanはほぼ同一の患者選択基準を使用しているので，AD発症の予測診断能についてFDG-PETの結果と比較することで脳血流SPECTの有用性と限界が明らかになる。

SEAD-JapanとJ-ADNIは重点の置き方に差異があるものの，共通してFDG-PETとMRIを評価の対象としている。SEAD-Japanでは参加施設が認知症のPETについて経験の豊富な9施設であり，画像検査としての品質管理が容易である。そのような施設からMCIのみを対象に症例を集め，主にAD発症の予測診断に目標を絞って主にFDG-PETの有用性を検討する研究であり，ADの早期診断に向けてのエビデンスの確立はSEAD-Japanで達成可能である。

一方，J-ADNIでは正常例，MCI，ADを網羅して多数例を集めるとともにAD発症の予測診断だけでなく，進行評価も対象にする。また，PET以上にMRIに重点が置かれるとともに，遺伝子検索を含む生物学的マーカーの確立も大きな柱であり，より網羅的な大規模研究である。PETについてはFDG-PETに加えてアミロイドイメージングも行うのでFDGとは性質の異なる画像を検討することになる。さらにJ-ADNIでは研究成果をより広く普及させるために画像検査の標準化，品質管理を大きな課題としている。

Ⅵ まとめ

J-COSMIC，SEAD-JapanはJ-ADNIの先行研究としてそれぞれ独自の意義を有しており，その成果が期待されるとともにJ-ADNIの実施につながる多くのノウハウを提供すると考えられる。

文 献

1）Silverman DH：Brain ^{18}F-FDG PET in the diagnosis of neurodegenerative dementias；Comparison with perfusion SPECT and with clinical evaluations lacking nuclear imaging. J Nucl Med 45：594-607，2004
2）Hirao K，Ohnishi T，Hirata Y，et al：The prediction of rapid conversion to Alzheimer's disease in mild cognitive impairment using regional cerebral blood flow SPECT. Neuroimage 28：1014-1021，2005
3）Drzezga A，Grimmer T，Riemenschneider M，et al：Prediction of individual clinical outcome in MCI by means of genetic assessment and (18)F-FDG PET. J Nucl Med 46：1625-1632，2005
4）Study on Diagnosis of early Alzheimer's disease-Japan ホームページ(http://square.umin.ac.jp/SEAD-J/)
5）Alzheimer's Disease Neuroimaging Initiative ホームページ(http://www.loni.ucla.edu/ADNI)

Eur Arch Psychiatry Clin Neurosci (2007) 257:473–479 DOI 10.1007/s00406-007-0750-2

ORIGINAL PAPER

Teruyasu Saze · Kazuyuki Hirao · Chihiro Namiki · Hidenao Fukuyama · Takuji Hayashi · Toshiya Murai

Insular volume reduction in schizophrenia

Received: 8 January 2007 / Accepted: 8 June 2007 / Published online: 27 September 2007

Abstract Structural and functional abnormalities of the insular cortex have been reported in patients with schizophrenia. Most studies have shown that the insular volumes in schizophrenia patients are smaller than those of healthy people. As the insular cortex is functio-anatomically divided into anterior and posterior subdivisons, recent research is focused on uncovering a specific subdivisional abnormality of the insula in patients with schizophrenia. A recent ROI-based volumetric MRI study demonstrated specific left anterior insular volume reduction in chronic schizophrenia patients (Makris N, Goldstein J, Kennedy D, Hodge S, Caviness V, Faraone S, Tsuang M, Seidman L (2006) Decreased volume of left and total anterior insular lobule in schizophrenia. Schizophr Res 83:155–171). On the other hand, our VBM-based volumetric study revealed a reduction in right posterior insular volume (Yamada M, Hirao K, Namiki C, Hanakawa T, Fukuyama H, Hayashi T, Murai T (2007) Social cognition and frontal lobe pathology in schizophrenia: a voxel-based morphometric study. NeuroImage 35:292–298). In order to address these controversial results, ROI-based subdivisional volumetry was performed using the MRI images from the same population we analyzed in our previous VBM-study. The sample group comprised 20 schizophrenia patients and 20 matched healthy controls. Patients with schizophrenia showed a global reduction in insular gray matter volumes relative to healthy comparison subjects. In a simple comparison of the volumes of each subdivision between the groups, a statistically significant volume reduction in patients with schizophrenia was demonstrated only in the right posterior insula. This study suggests that insular abnormalities in schizophrenia would include anterior as well as posterior parts. Each subdivisional abnormality may impact on different aspects of the pathophysiology and psychopathology of schizophrenia; these relationships should be the focus of future research.

Key words schizophrenia · insular · volumetry · self-awareness

T. Saze, MD (✉) · K. Hirao, MD · C. Namiki, MD
T. Hayashi, MD, PhD · T. Murai, MD, PhD
Department of Neuropsychiatry
Graduate School of Medicine
Kyoto University
Kyoto 606-8507, Japan
Tel.: +81-75-7513382
Fax: +81-75-7513246
E-Mail: sazeteru@kuhp.kyoto-u.ac.jp

C. Namiki, MD · H. Fukuyama, MD, PhD
Human Brain Research Center
Graduate School of Medicine
Kyoto University
Kyoto 606-8507, Japan

Introduction

It has been postulated that dysfunction of the limbic system would be linked to difficulties in distinguishing between internal and external perceptions and regulating behaviors, ultimately allowing the emergence of the psychotic symptoms of schizophrenia; however, the underlying pathology remains to be elucidated [2, 9, 27]. The insular cortex is part of the limbic region, playing a key role in integrating perceptual experiences and affects to produce balanced behavior [1, 16].

There is converging evidence of a functio-anatomical abnormality of the insula in patients with schizophrenia. Functional neuroimaging studies suggest that insular hypometabolism [6] or decreased cerebral blood flow [4] might be involved in the pathophysiology of schizophrenia. Volumetric magnetic resonance imaging (MRI) studies of the insular cortex have almost unanimously indicated that there are morphological abnormalities of the insular gray matter in patients with schizophrenia [7, 10, 14, 18–21, 24, 25, 27].

EAPCN 750

However, what remains unsolved is whether the insular abnormality in schizophrenia is specific to a certain subdivision (or lateralized), or if it is bilateral and global. Regarding the laterality issue, the literature is inconsistent: some studies report bilateral insular volume reductions [10, 14, 20, 25], whereas others report left-sided volume reductions [19, 21, 24]. Right-sided insular volume reduction has also been reported in female subjects [7].

In addition to the laterality issue, what is important is the intrahemispheric functio-anatomical subdivision of the insular cortex. The insular cortex is anatomically divided into two major subdivisions (anterior and posterior lobules) by the central sulcus of the insula [22, 23]. Morphological separation between these two parts reflects, to some extent, the characteristics of the cytoarchitectonic composition and their different neural connections. The anterior insula represents the agranular and adjacent dysgranular insula, and is connected to the piriform, orbitofrontal, temporopolar and parahippocampal regions. Together with the above-mentioned areas, the anterior insula plays a role in the control of emotions and autonomic regulation. By contrast, the posterior insular lobule consists of the granular and adjacent regions, and is more closely connected to the somatosensory, auditory, and motor areas [17]. The posterior insula mainly connects with the primary and secondary somatosensory cortices (SI, SII), the superior and inferior parietal lobules, the orbitofrontal, prefrontal and premotor cortices, the auditory cortex (AI, AII), the superior and inferior temporal cortices, the basal ganglia and the thalamus [1, 17].

Makris et al. [15] recently measured the volumes of the insular subregions (left/right × anterior/posterior) using the central sulcus of the insula as a landmark for subdivisions, and investigated the volumetric alteration of the insula in patients with schizophrenia based on a volumetric MRI study. The authors reported that there was a significant reduction in insular cortical volume throughout the anterior insular lobules, and particularly in the left anterior lobule, in chronic schizophrenia patients compared with normal controls.

However, there are technical problems in previous volumetric MRI studies. Since the insula is a relatively small structure, it is difficult to clearly delineate it in images of low spatial resolution, especially when subdivisional volumetry is intended. Most studies have utilized lower magnetic field MR images (from 1.0 to 1.5 T) and obtained slices thicker than 1 mm (~1.5–3 mm). Such low quality protocols might lead to insufficient measurement of insular volumes.

Previously, our voxel-based morphometry (VBM) study revealed that there is a volume reduction in the right posterior insular lobules of patients with schizophrenia [26], in contrast to the results of Makris et al. [15]. Thus, to address these controversial results, a region-of-interest (ROI)-based subdivisional volumetry study was performed using the MRI images from the same population we analyzed in our previous VBM-study [26]. The analyzed structural MRI images were obtained using a 3.0 T MRI scanner with slices of an acceptable thickness (1 mm) to investigate changes in the volumes of the subdivisions of the insular cortex.

Methods

Participants

The participants are identical to those of our previous study [26]. The schizophrenia group comprised 20 patients (10 men and 10 women), referred to the Department of Psychiatry, Kyoto University Hospital. Exclusion criteria included a history of seizure disorder, head trauma resulting in a loss of consciousness, neurological illness or substance abuse. Based on the Structural Clinical Interview for DSM-IV (SCID), all patients met DSM-IV criteria for schizophrenia and clinical symptoms were rated according to the Positive and Negative Syndrome Scale (PANSS; [13]). All patients were being treated with antipsychotic medications and were physically healthy at the time of scanning. Haloperidol equivalents, which were calculated according to Inagaki et al. [11], were administered at 11.9 ± 8.9 mg/day. Among the 20 patients, 18 were being treated with atypical antipsychotic medications (12 with 6.63 ± 3.45 mg/day of risperidone, 5 with 10.00 ± 6.12 mg/day of olanzapine, 3 with 391.7 ± 278.8 mg/day of quetiapine, and 2 with 18.00 ± 6.00 mg/day of perospirone): 11 were being treated with a single atypical antipsychotic medication, three were being treated with multiple atypical antipsychotics, and four were being treated with atypical antipsychotics in combination with typical (haloperidol or chlorpromazine) antipsychotics. Two patients were being treated with multiple typical antipsychotics. Some patients (n = 8) were also receiving adjunctive anticholinergic treatment. The comparison group comprised 20 healthy individuals (10 men and 10 women) who were matched with the schizophrenia group with regard to age and education level. These subjects were also evaluated on the basis of SCID. They had no current or past history of psychiatric or neurologic diseases. In addition, they had no first degree relatives who had current or past psychotic episodes.

Table 1 indicates the demographic characteristics of the two groups. The estimated verbal and performance IQs were obtained from vocabulary and block design subtasks, respectively, using the Wechsler Adult Intelligence Scale-Revised (WAIS-R) by transforming the scores corrected for age into T scores.

After a complete description of the study to the participants, they gave written informed consent to a protocol approved by the Committee on Medical Ethics of Kyoto University.

MRI acquisition and pre-processing

MR images were obtained at Kyoto University Hospital on a 3-T whole-body scanner equipped with an 8-channel phased array coil (Trio, Siemens, Erlangen, Germany). The scanning parameters of the three-dimensional magnetization-prepared rapid gradient-echo (3D-MPRAGE) sequences were as follows: TE = 4.38 ms; TR = 2000 ms; TI = 990 ms; FOV = 240; slice plane = axial; slice thickness = 1 mm; resolution = 0.94 × 0.94 × 1.0; and slice number = 208. In order to increase the signal/noise ratio, we scanned all participants three times and obtained average images from the three scans using statistical parametric mapping 2 (SPM2) software (The Wellcome Department of Imaging Neuroscience, London, U.K.) running in Matlab 6.5 (The Math Works, Natic, MA, U.S.).

Table 1 Demographic, clinical, and neuropsychological characteristics of the subjects

	Schizophrenia ($n = 20$)		Healthy ($n = 20$)		Statistics	
	Mean	S.D.	Mean	S.D.	t (df. = 38)	p
Age (years)	38.8	7.2	39.1	7.1	0.13	$p > 0.05$
Sex (male/female)	10/10		10/10		–	–
Handedness (right/left)	19/1		19/1		–	–
Education years	13.5	2.0	14.4	1.9	0.15	$p > 0.05$
Age at onset (years)	27.4	6.4	–	–	–	–
Duration of illness (years)	11.6	8.7	–	–	–	–
Drug (mg/day, haloperidol equivalent)	11.9	8.9	–	–	–	–
PANSS Total	64.5	19.8	–	–	–	–
PANSS Positive	16.4	6.7	–	–	–	–
PANSS Negative	15.7	6.5	–	–	–	–
PANSS General	32.4	10.1	–	–	–	–
VIQ	97.8	16.0	107.5	14.8	2.00	$p > 0.05$
PIQ	97.8	14.9	107.0	12.7	2.11	$p = 0.04$

ROI definition

The boundaries of the insular cortex were manually determined using MRIcro (Chris Rorden, University of Nottingham, Great Britain) on consecutive coronal slices. The most rostral coronal plane containing the insular cortex and the coronal plane containing the fusion of the superior and inferior circular insular sulci were chosen as anterior and posterior boundaries, respectively. On each coronal slice, the insular cortex was bounded superiorly by the superior circular insular sulcus, and inferiorly by the inferior circular insular sulcus or the orbitoinsular sulcus, following the procedure of Crespo-Facorro et al. [3]. In addition, following the procedure applied by Makris et al. [15], the central sulcus of the insula was considered as the landmark dividing the insular cortex into anterior and posterior parts; thus, this sulcus constitutes the inferior border of the anterior insular lobule and the superior border of the posterior insular lobule (Fig. 1). The volume of each lobule was calculated by multiplying the number of voxels assigned to that structure by the single-voxel volume $0.94 \times 0.94 \times 1.0$ mm^3. All measurements were carried out by the first author (TS) who was blind to subjects' identity, demographic data, diagnosis, and psychopathology.

To determine the reliability of the insular measurements, 10 subjects were randomly selected. Segmentation and parcellation was independently carried out by the first author and another researcher who was experienced at volumetric analysis. Both raters were blinded to participant details, including the study group and

Figure 1 The anterior and posterior insular lobules

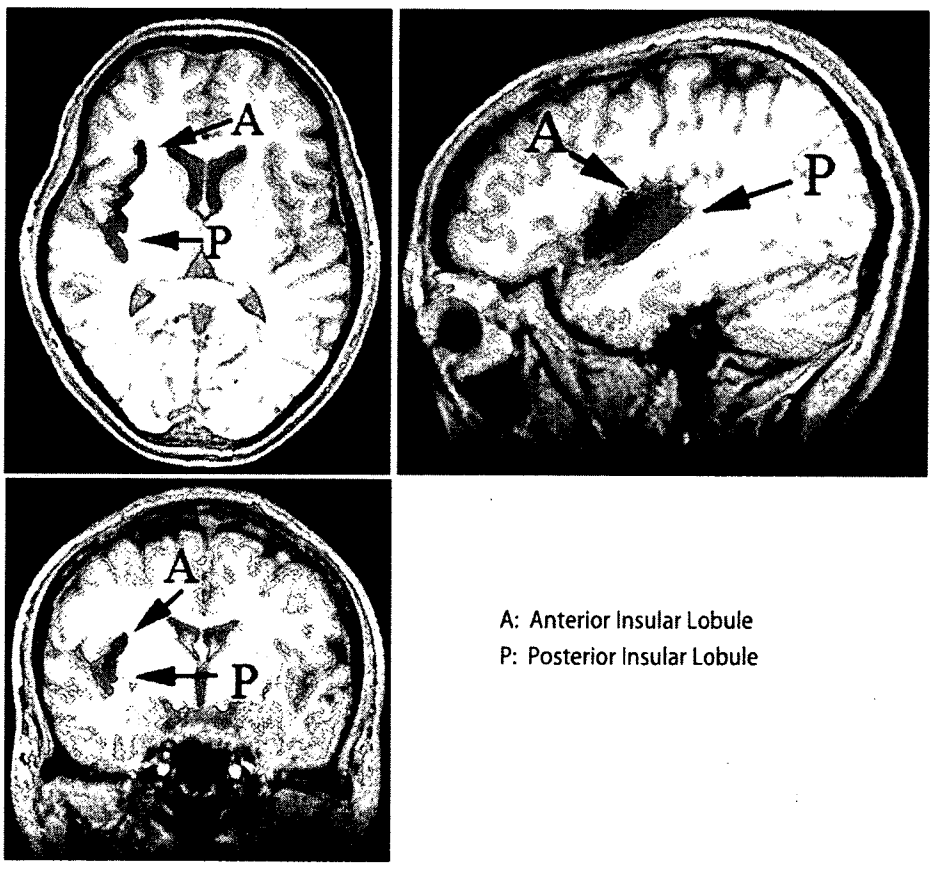

the results of neuropsychological tests, during the measurement. For the insula subregion, intrarater reliability ranged from 0.96 to 0.97; interrater reliability ranged from 0.90 to 0.92 using Cronbach's alpha coefficient.

Intracranial volume (ICV) measurement

Estimates of the global gray and white matter volumes and cerebrospinal fluid (CSF) volume were obtained after the automatic brain segmentation procedure had been carried out by SPM2 in our previous study [26]. Total ICV was the sum of the volumes of gray and white matters and CSF.

Statistical analysis

In group comparisons of the insular subdivisional gray matter volumes, the relative volume ([absolute ROI volume/ICV] × 100) was analyzed by repeated measures analysis of variance (ANOVA) with group (schizophrenia, control) as a between-subject factor, and hemisphere (left, right) and subregion (anterior, posterior) as within-subject variables. As mentioned in the introduction, each insular subdivision differs in its anatomical features, connectivity and functional roles. Thus, we were also interested in determining if the volumes of each insular subdivision differ significantly between the groups, especially for those of the left anterior and right posterior subdivisions, the volumes of which have been reported to be reduced in schizophrenia patients [15, 26]. Hence, separate group comparisons for each of the four subregional volumes were performed without correction for multiple comparisons of the four subregions.

Finally, in order to investigate the relationship between the gray matter volumes of the patients' insular subregions and their PANSS scores, parametric statistics were used if an initial exploration of the data set indicated a normal distribution; otherwise nonparametric statistics were applied.

For all of the resulting statistics, the significance threshold was set at $p < 0.05$. All of the above statistical analyses were performed using SPSS v.12.0.

Results

Demographic and clinical characteristics of patients and controls

Demographic and clinical data are summarized in Table 1. Two-tailed t-tests were applied to compare the differences in demographic and clinical variables between groups. The groups did not differ significantly in age, sex, handedness, education or estimated VIQ. The estimated PIQs of the schizophrenia subjects were significantly worse than those of healthy controls [controls = 107.0 (12.7); patients = 97.8 (14.9); $t = 2.11$; df = 38; $p = 0.04$].

Volume change

The ANOVA revealed a significant main effect of group ($F = 4.280$, df = 38, $p = 0.045$), subregion ($F = 677.4$, df = 38, $p < 0.001$) and a hemisphere-by-subregion interaction ($F = 8.825$, df = 38, $p = 0.005$), but no significant main effect of hemisphere ($F = 0.019$, df = 38, $p = 0.890$) and no significant group-by-hemisphere ($F = 0.086$, df = 38, $p = 0.771$), group-by-subregion ($F = 0.041$, df = 38, $p = 0.840$), or group-by-hemisphere-by-subregion ($F = 1.027$, df = 38, $p = 0.317$) interactions. This result suggests that patients with schizophrenia have a global (that is, non-specific to subregion or hemisphere) reduction in the volume of insular gray matter relative to healthy subjects. When subregional relative volumes were compared between groups separately, a significant difference was demonstrated only in the right posterior lobule ($F = 4.960$, df = 38, $p = 0.032$), but not in the other three subregions (Table 2 and Fig. 2).

Table 2 Insular volumes in subjects with schizophrenia and healthy controls

	Schizophrenia ($n = 20$)		Healthy ($n = 20$)		Statistics	
	Mean	S.D.	Mean	S.D.	t (df = 38)	p
Intracranial volume (ml)	1564.1	212.8	1617.3	172.3	0.87	0.39
Insular cortex volume						
Right anterior						
Absolute (ml)	3.5	0.59	3.5	0.35		
Relative (%)	0.23	0.029	0.22	0.027	−1.00	0.33
Right posterior						
Absolute (ml)	1.9	0.40	1.8	0.30		
Relative (%)	0.13	0.021	0.11	0.015	−2.20	0.032
Left anterior						
Absolute (ml)	3.7	0.59	3.6	0.47		
Relative (%)	0.24	0.029	0.22	0.026	−1.50	0.13
Left posterior						
Absolute (ml)	1.8	0.33	1.7	0.19		
Relative (%)	0.11	0.017	0.11	0.015	−1.20	0.24

Correlations between volumes and clinical measures

Age, age when first medicated, duration of medication treatment, or current dose of antipsychotic medication, were not correlated with any of the investigated relative volumes. No significant correlation was demonstrated between any of the investigated relative volumes and any of the three PANSS subscores (positive, negative and general scores).

Discussion

Three main findings emerge from this study: (1) schizophrenia patients show a global reduction in insular volumes; (2) among insular subregions, the right posterior insula was the only subregion in which patients showed a significant volume reduction; (3) in the patient group, none of the subregional insular volumes were associated with psychopathological measures.

Insular volume reduction in schizophrenia

Although, most previous studies have shown volume reduction in the insular gray matter in patients with schizophrenia, little is known regarding the subdivi-

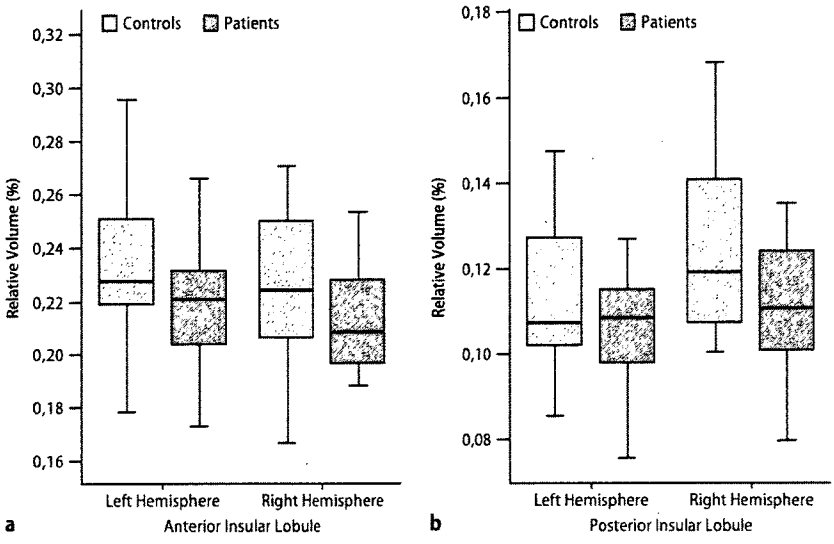

Figure 2 Box-plots of the relative volumes (%) of the insular lobules in the anterior (**a**) and posterior (**b**) zones of patients with chronic schizophrenia (n = 20) and healthy control subjects (n = 20). Means are indicated by horizontal lines. Each box encompasses 50% of the distribution of volumes

sional specificity of this volume reduction, as summarized in the Introduction. Our results, using high spatial resolution images, suggest that the insular abnormality is not subregion specific, but global, affecting the structure bilaterally as well as in both anterior and posterior subregions. Thus, the inconsistencies of the previous literature might be due to differences in patient characteristics as well as substantial measurement error variations associated with lower resolution images.

Specifically, in contrast to the recent study by Makris et al. [15], which is, other than our studies, the only study to investigate the insular subregional volumes in schizophrenia by dividing the insula into anterior and posterior sections, we did not demonstrate a specific volume reduction in the left anterior insula. This discordance might originate from differences in the characteristics of the patients investigated; for example, the illness durations in the patients in Makris' study (22.5 ± 10.9 years) were twice as long as those in ours (11.6 ± 8.7 years). However, the difference in methodological protocols would also be important. We traced an average of 50 coronal slices per subject when measuring the insular cortex; among these, 30 covered the posterior insular cortex. We believe that this method, using 1 mm-thick slices, can provide a more exact measure of the subregional volumes than that of Makris et al. [15], using 3 mm-thick coronal slices.

Although we did not demonstrate a statistically significant group difference in left anterior insular volumes, our assertion is not that the left anterior insula is not involved in the pathophysiology of schizophrenia, but that the left anterior insula is not specifically involved. Anterior and posterior subdivisions of the insula are involved in different neural circuitries, and bear a differential impact on our cognition and behavior. We suspect that the functions of both subdivisions would be compromised in schizophrenia. Pathology of the anterior insula, together with other limbic and paralimbic structures, mainly affects emotional processes modulating our behaviors. Pathology of the posterior subdivision would have a different impact.

Regarding the effect of medication on regional volumes, we found no significant correlation between antipsychotic doses and subdivisional insular volumes. Dazzan et al. [5] reported that typical but not atypical antipsychotics are likely to induce regional cortical volume reductions, including a volume reduction in the insula, among first episode schizophrenia patients. The lack of an association of medication with insular volumes in our current study might be due to the fact that most of the patients were being treated with atypical antipsychotics.

The volume change in the right posterior lobule

The main result of our analysis should be interpreted as a global reduction in the volume of the insula. However, in a separate group comparison for each subdivision, the only subregion in which a significant difference in volumes was found was the right posterior insula, although this difference was marginal without correction for multiple comparisons. Comparing the methodological advantages and disadvantages of VBM and manual ROI analysis, Kubicki et al. [14] recommended the initial use of VBM in an exploratory manner and subsequent confirmatory analyses by application of manual ROI tracing. Such an approach has been demonstrated to be successful in our analysis regarding the insular cortical volumes of schizophrenia: an initial whole-brain VBM analysis revealed a reduced volume region in the right posterior part of the insula [26], and this preliminary result was further confirmed by the present analysis using manual ROI tracing.

Although not fully elucidated, recent neuroimaging studies provide a clue to the possible functional sig-

nificance of this particular subregion of the human insula. Based on a lesion study analyzing an unselected sample of stroke patients with right brain damage, Karnath et al. [12] reported that right posterior insula lesions are specifically associated with "anosognosia" for hemiplegia/hemiparesis. On the other hand, in an activation study by Farrer et al. [8] using positron emission tomography (PET), healthy subjects were requested to indicate whether movements they saw on a computer screen corresponded to their executed movements, or were controlled by another person. The experiment showed decreased activity in the right posterior insula with a decreasing feeling of controlling the movement; that is, when subjects experienced a mismatch between what they did and what they saw. By contrast, this activity was increased when the afferent input matched their own actions. A possible interpretation of these findings is that the right posterior insula plays an important role in integrating signals related to self-awareness and establishing a boundary between self and others.

Although speculative, considering the functional significance of this region, some of the core characteristics of the psychopathology of schizophrenia could be explained by a dysfunctional right posterior insula: lack of insight could be explained straightforwardly as compromised self-awareness, while multimodal hallucinations could also be interpreted as a consequence of misintegration of sensory inputs into self-awareness.

Unfortunately, we did not find any correlation between psychopathological measures and the volume of any of the insular subregions, including the right posterior insula. The small sample size or non-uniformity of the subjects investigated (including both first episode subjects and more chronic subjects) might have affected our results of non-association between psychopathology and insular volumes. However, previous studies are also controversial regarding the association of psychopathology and insular volume reduction. If the above-mentioned role of the right posterior insula and its possible impact on psychopathology are true, such a putative association could be demonstrated using specifically-designed cognitive tasks or psychopathological measures to capture aspects of self-awareness in schizophrenia; this is the goal of our future studies.

Acknowledgments This work was supported by the Uehara Memorial Foundation, the Kobayashi Magobe Memorial Medical Foundation, and the Research Group for Schizophrenia, Japan.

References

1. Augustine JR (1996) Circuitry and functional aspects of the insular lobe in primates including humans. Brain Res Rev 22:229–244
2. Brebion G, Smith MJ, Amador X, Malaspina D, Gorman JM (1998) Word recognition, discrimination accuracy, and decision bias in schizophrenia Association with positive symptomatology and depressive symptomatology. J Nerv Ment Dis 186:604–609
3. Crespo-Facorro B, Kim JJ, Andreasen NC, O'leary DS, Bockholt J, Magnotta V (2000) Insular cortex abnormalities in schizophrenia: a structural magnetic resonance imaging study of first-episode patients. Schizophr Res 46:35–43
4. Curtis VA, Bullmore ET, Brammer MJ, Wright IC, Williams SC, Morris RG, Sharma TS, Murray RM, McGuire PK (1998) Attenuated frontal activation during verbal fluency tasks in patients with schizophrenia. Am J Psychiatry 155:1056–1063
5. Dazzan P, Morgan KD, Orr K, Hutchinson G, Chitnis X, Suckling J, Fearon P, McGuire PK, Mallett RM, Jones PB, Leff J, Murray RM (2005) Different effects of typical and atypical antipsychotics on grey matter in first episode psychosis: the AESOP study. Neuropsychopharmacology 30:765–774
6. Desco M, Gispert J, Reig S, Sanz J, Pascau J, Sarramea F, Benito C, Santos A, Palomo T, Molina V (2003) Cerebral metabolic patterns in chronic and recent-onset schizophrenia. Psychiatry Res Neuroimaging 122:125–135
7. Duggal HS, Muddasani S, Keshavan MS (2005) Insular volumes in first-episode schizophrenia: gender effect. Schizophr Res 73:113–120
8. Farrer C, Franck N, Georgieff N, Frith CD, Decety J, Jeannerod M (2003) Modulating the experience of agency: a positron emission tomography study. NeuroImage 18:324–333
9. Frith C, Dolan RJ (1997) Brain mechanisms associated with top-down processes in perception. Philos Trans R Soc Lond B Biol Sci 352:1221–1230
10. Hulshoff Pol HE, Schnack HG, Mandl RCW, Haren NEM, Konig H, Collins L, Evans AC, Kahn RS (2001) Focal gray matter density changes in schizophrenia. Arch Gen Psychiatry 58:1118–1125
11. Inagaki A (2004) Translation table of psychotropic drugs. Keio University, Tokyo
12. Karnath HO, Baier B, Nagele T (2005) Awareness of the functioning of one's own limbs mediated by the insular cortex? J Neurosci 25:7134–7138
13. Kay SR, Fiszbein A, Opler LA (1987) The Positive and Negative Syndrome Scale (PANSS) for schizophrenia. Schizophr Bull 13:261–276
14. Kubicki M, Shenton ME, Salisbury DF, Hirayasu Y, Kasai K, Kikinis R, Jolesz FA, McCarley RW (2002) Voxel-based morphometric analysis of gray matter in first episode schizophrenia. NeuroImage 17:1711–1719
15. Makris N, Goldstein J, Kennedy D, Hodge S, Caviness V, Faraone S, Tsuang M, Seidman L (2006) Decreased volume of left and total anterior insular lobule in schizophrenia. Schizophr Res 83:155–171
16. Mesulam MM, Mufson EJ (1982) Insula of the old world monkey: III. Efferent cortical output and comments on function. J Comp Neurol 212:38–52
17. Mesulam MM, Mufson EJ (1985) The insula of Reil in man and monkey Architectonics connectivity and function. In: Peters A, Jones EG (eds) Cerebral cortex, vol 4. Association and auditory cortices. Plenum Press, New York, pp 179–226
18. Okugawa G, Tamagaki C, Agartz I (2007) Frontal and temporal volume size of grey and white matter in patients with schizophrenia : an MRI parcellation study. Eur Arch Psychiatry Clin Neurosci 257:304–307
19. Paillere-Martinot M, Caclin A, Artiges E, Poline JB, Joliot M, Mallet L, Recasens C, Attar-Levy D, Martinot JL (2001) Cerebral gray and white matter reductions and clinical correlates in patients with early onset schizophrenia. Schizophr Res 50:19–26
20. Shapleske J, Rossell SL, Chitnis XA, Suckling J, Simmons A, Bullmore ET, Woodruff PWR, David AS (2002) A computational morhpometric MRI study of schizophrenia: effect of hallucinations. Cereb Cortex 12:1331–1341

21. Sigmundsson T, Suckling J, Maier M, Williams SCR, Bullmore ET, Greenwood KE, Fukuda R, Ron MA, Toone BK (2001) Structural abnormalities in frontal, temporal, and limbic regions and interconnecting white matter tracts in schizophrenic patients with prominent negative symptoms. Am J Psychiatry 158:234–243
22. Ture U, Yasargil DC, Al-Mefty O, Yasargil MG (1999) Topographic anatomy of the insular region. J Neurosurg 90:720–733
23. Varnavas GG, Grand W (1999) The insular cortex: morphological and vascular anatomic characteristics. Neurosurgery 44:127–136 (discussion 136–138)
24. Wilke M, Kaufman C, Grabner A, Putz B, Wetter TC, Auer DP (2001) Gray matter-changes and correlates of disease severity in schizophrenia: a statistical parametric mapping study. NeuroImage 13:814–824
25. Wright IC, Ellison ZR, Sharma T, Friston KJ, Murray RM, McGuire PK (1999) Mapping of grey matter changes in schizophrenia. Schizophr Res 35:1–14
26. Yamada M, Hirao K, Namiki C, Hanakawa T, Fukuyama H, Hayashi T, Murai T (2007) Social cognition and frontal lobe pathology in schizophrenia: A voxel-based morphometric study. NeuroImage 35:292–298
27. Yamasaki S, Yamasue H, Abe O, Yamada H, Iwanami A, Hirayasu Y, Nakamura M, Furukawa SI, Rogers MA, Tanno Y, Aoki S, Kato N, Kasai K (2007) Reduced planum temporale volume and delusional behaviour in patients with schizophrenia. Eur Arch Psychiatry Clin Neurosci (in press)

Temporal Change in Human Nicotinic Acetylcholine Receptor After Smoking Cessation: 5IA SPECT Study

Marcelo Mamede[1], Koichi Ishizu[1], Masashi Ueda[2], Takahiro Mukai[1], Yasuhiko Iida[2], Hidekazu Kawashima[2], Hidenao Fukuyama[3], Kaori Togashi[1], and Hideo Saji[2]

[1]Department of Diagnostic Imaging and Nuclear Medicine, Graduate School of Medicine, Kyoto University, Kyoto, Japan; [2]Department of Patho-Functional Bioanalysis, Graduate School of Pharmaceutical Science, Kyoto University, Kyoto, Japan; and [3]Brain Function Imaging Division, Human Brain Research Center, Graduate School of Medicine, Kyoto University, Kyoto, Japan

Nicotinic acetylcholine receptors (nAChRs) are of great interest because they are implicated in various brain functions. They also are thought to play an important role in nicotine addiction of smokers. Chronic (−)-nicotine, a nAChR agonist, treatment in mice and rats elicits a dose-dependent increase in nAChRs in the brain. Upregulation of nAChRs in postmortem human brains of smokers has also been reported. However, changes in nAChRs after cigarette smoking cessation in humans are poorly understood. The aim of this study was to detect the dynamic changes of nAChRs after smoking and smoking cessation in the brains of living subjects. **Methods:** We performed 5-^{123}I-iodo-A-85380 (^{123}I-5IA) SPECT on nonsmokers and smokers (n = 16) who had quit smoking for 4 h, 10 d, and 21 d and calculated and compared distribution volumes (Vt) of ^{123}I-5IA. **Results:** The binding potential of nAChRs (Vt of ^{123}I-5IA) in the brains of smokers decreased by 33.5% ± 10.5% after 4 h of smoking cessation, increased by 25.7% ± 9.2% after 10 d of smoking cessation, and decreased to the level of nonsmokers after 21 d of smoking cessation. **Conclusion:** Because the upregulation of the nAChRs of the smokers after chronic exposure of the nicotine was downregulated to the nonsmokers' level by around 21 d after smoking cessation, the upregulation is a temporary effect. The decrease in nicotinic receptors to nonsmoker levels may be the breaking point during the nicotine withdrawal period.

Key Words: ^{123}I-5IA; SPECT; nicotinic acetylcholine receptors; human brain; smoking withdrawal; quantitative measurement

J Nucl Med 2007; 48:1829–1835
DOI: 10.2967/jnumed.107.043471

Nicotinic acetylcholine receptors (nAChRs) are a family of ligand-gated ion channels that regulate neurotransmission in the central and peripheral nervous systems. These receptors are of great interest because they are implicated in various brain functions, including cognition and memory (*1,2*) and in nicotine-induced neuroprotective (*3*) and analgesic effects (*4*). In addition, these receptors are thought to play an important role in nicotine addiction (*5*).

Chronic treatment with agonists for most neurotransmitter receptor systems results in a decrease in receptor number. However, it has been demonstrated that chronic treatment of mice (*6*) and rats (*7*) with (−)-nicotine, an nAChR agonist, elicits a dose-dependent increase in nAChRs. This upregulation is not permanent, returning to control levels within 7–10 d in mice (*6*) and 15–20 d in rats (*8,9*) after cessation of (−)-nicotine treatment. Previous efforts to demonstrate nAChR upregulation in the human brain have also been reported primarily in in vitro binding assays (*10,11*). Kassiou et al. reported the upregulation of nAChRs with chronic (−)-nicotine treatment in the brain of a live baboon (*12*). More recently, Staley et al. described the upregulation of nAChRs in human brains after early abstinence of tobacco smoking using 5-^{123}I-iodo-A-85380 (^{123}I-5IA) and SPECT images (*13*). However, changes in nAChRs in humans after cessation of smoking are poorly understood. Breese et al. studied the levels of ^{3}H-nicotine binding in humans postmortem for changes in nicotinic receptor levels and reported that the nAChR levels in smokers who had stopped smoking at least 2 mo before their death were similar to those in nonsmokers (*14*); the effects of shorter-term smoking cessation are unknown.

^{123}I-5IA is a nAChR imaging probe that has extremely high selectivity and specificity for the α4β2 subunit of nAChRs in rodent (inhibition constant = 0.37 nM) (*15*) and primate brain in vivo (*16*), with relatively low acute toxicity (effective dose equivalent = 30 μSv/MBq) (*17,18*). Moreover, we have developed the methodology for the quantification of nAChRs in human brain using ^{123}I-5IA and SPECT (*19*).

The aim of the present study was to detect the dynamic changes of nAChRs in living human brain after smoking and smoking cessation. We performed ^{123}I-5IA SPECT on nonsmokers and smokers who had quit smoking for 4 h, 10 d, and

Received May 9, 2007; revision accepted Jul. 30, 2007.
For correspondence or reprints contact: Koichi Ishizu, MD, PhD, Department of Diagnostic Imaging and Nuclear Medicine, Graduate School of Medicine, Kyoto University, Sakyo, 606-8507, Kyoto, Japan.
E-mail: ishizu@kuhp.kyoto-u.ac.jp
COPYRIGHT © 2007 by the Society of Nuclear Medicine, Inc.

21 d and compared the distribution volumes (*Vt*) of ^{123}I-5IA of each group and with nonsmokers. To our knowledge, this is the first in vivo imaging study of nAChR upregulation and recovery in response to short-term smoking cessation in living subjects.

MATERIALS AND METHODS

Volunteers

Six male nonsmokers (23 ± 6 y) and 10 healthy male smokers (28 ± 4 y) were included in this study. Five smokers in the 4-h group were also included in either the 10-d or the 21-d group. In total, 21 ^{123}I-5IA SPECT studies were acquired (Table 1). None of the subjects had a history of neurologic or psychiatric illness or the use of psychotropic or sleep-inducing drugs. The nonsmokers had no history of smoking tobacco.

For the smoking withdrawal studies, the smokers were divided in 3 groups: 5 subjects (age, 28 ± 4 y) for 4-h withdrawal, 5 subjects (age, 27 ± 6 y) for 10-d withdrawal, and 5 subjects (age, 28 ± 3 y) for 21 d of smoking withdrawal. The 4 groups were age-matched.

All subjects gave written informed consent to participate in this study in compliance with the regulations of the Joint Committee on Clinical Investigation of the Kyoto University Hospital.

Radiolabeling

Radiolabeling of the ^{123}I-5IA followed the methods we reported previously (*19*). To a sodium ^{123}I-iodide solution (1,110 MBq) (Nihon Medi-Physics), 100 μg of (*S*)-5-(tri-*n*-butylstannyl)-3-([1-*t*-butoxycarbonyl-2(*S*)-azetidinyl]methoxy)pyridine, 1.5% acetic acid, 3 mol/L HCl, and 5% H_2O_2 solution were added, and the mixture was stirred at 75°C for 15 min. Concentrated HCl was then added, and the resulting solution was stirred for another 10 min at 75°C. The mixture was made basic with NaOH and extracted with ethyl acetate, and the organic layer was evaporated. The residue was purified by reverse-phase high-performance liquid chromatography ([HPLC] Cosmosil 5C18-AR-300, 10 × 250 mm; Nacalai Tesque; 10 mmol/L ammonium acetate/methanol/triethylamine = 752:750:2; 1.5 mL/min; retention time for 5IA was 40 min). After evaporation of the HPLC eluent, the residue was dissolved in 0.9% saline and filtered through a 0.2-μm filter into a sterile vial. Radiochemical purity was >98%, and radiochemical yields were ~42%. The specific activity determined from the ultraviolet absorbance at 254 nm was >169 GBq/μmol (the detection limit for this method).

SPECT

All subjects underwent a set of 5 SPECT dynamic scans (a 120-min scan, followed by 4 sets of 20-min scans). All SPECT dynamic scans were acquired with a triple-head rotating γ-camera system (PRISM 3000; Picker International) equipped with low-energy, high-resolution, fanbeam collimators. Data acquisition and image reconstruction were performed as in our previous study (*19*). The data acquisition was alternately performed over 120 min after intravenous injection of ^{123}I-5IA, followed by 4 sets of 20-min scans (at 3, 4, 5, and 6 h after the injection). SPECT images were reconstructed using a filtered backprojection algorithm with a ramp filter. Attenuation correction was performed using ellipses outer line approximation and Chang's method (coefficient of 0.06/cm), which assumes that the attenuation process is homogeneous throughout the brain and can be described by an exponential function. Scatter correction was not applied.

A dose of ~150 MBq of ^{123}I-5IA was administered intravenously over a period of 1 min at a constant rate with an infusion pump, and the SPECT scan was started at the same time as the injection. Arterial blood sampling and metabolite correction were also performed to estimate the arterial input function of the ^{123}I-5IA for each volunteer by the same method as that used in our earlier study (*19*).

TABLE 1
Study Groups

Nonsmokers	Smokers: period of smoking cessation		
	4 h	10 d	21 d
Subject 1	Subject 7	Subject 7	Subject 9
Subject 2	Subject 8	Subject 8	Subject 10
Subject 3	Subject 9	Subject 12	Subject 11
Subject 4	Subject 10	Subject 13	Subject 15
Subject 5	Subject 11	Subject 14	Subject 16
Subject 6			

Arterial Input Function

Twenty-five arterial blood samples were obtained at the same time points as described previously (*19*). From each sample, 100 μL of plasma were removed and the radioactivity was measured in an automatic well-type γ-counter (Cobra 2; Packard Instruments). Sixteen samples were analyzed by thin-layer chromatography (TLC) (10% ammonium acetate and methanol [1:1], LK6DF Silica Gel, 60 Å; Whatman) for metabolite determination (R_f = 0.55 for ^{123}I-5IA) (*19*). The measured unmetabolized fractions were fitted with a dual exponential curve, and the input function was calculated as all plasma sample counts were corrected for metabolites using the fitted curve.

Data Analysis

Reconstructed SPECT images were automatically coregistered using a coregistration algorism of statistical parametric mapping, SPM99 (Welcome Department of Cognitive Neurology, London, U.K.), to minimize positional error caused by head movement during the scans. Multiple circular regions of interest (ROIs) (21 pixels per circle) were manually drawn in each brain region (basal ganglia, thalamus, brain stem, cerebellum, frontal, parietal, temporal, and occipital cortices) on both sides. ROI data were further decay-corrected. SPECT data were calibrated to the well counter used to measure the injected activity. Time–activity curves were generated from the ROIs and the dynamic image datasets.

Kinetic analysis of the ^{123}I-5IA was performed using a 2-compartment model including K_1 and k_2 rate constants and a curve-fitting method following our previous study (*19*). *Vt* values of the ^{123}I-5IA were calculated and used as a quantitative index correlated with the regional binding potential of the nAChRs. The *Vt* values were further evaluated in terms of interval change after the smoking withdrawal.

Statistical Analysis

All data are expressed as the mean ± SD. The *Vt* values obtained from the different regions in the brain were analyzed by 1-way ANOVA with the Bonferroni protected least significant difference test. The interval changes of the ^{123}I-5IA *Vt* were analyzed between the 3 phases after the smoking withdrawal using the Tukey–Kramer multiple comparison test. All tests were 2-sided, and probability values of $P < 0.05$ were considered significant.

RESULTS

As in our previous study (*19*), the characteristics of the arterial input functions for all volunteers (nonsmokers and smokers) were similar. The peak plasma activity occurred between 70 and 80 s after injection in all subjects and decreased rapidly to 6.5%–9.0% of the peak level in 10 min. Analysis of the unmetabolized compound by TLC demonstrated a high parent fraction of ^{123}I-5IA in the plasma (87.7% ± 6.3%) in the first minute. ^{123}I-5IA was rapidly metabolized, and the unchanged fraction represented 50.9% ± 8.8% and 32.4% ± 12.6% of total plasma activity at 20 and 60 min, respectively.

Figure 1 shows the representative standardized time–activity curve of ^{123}I-5IA in the frontal cortex. The concentrations of radioactivity were slightly higher in the nonsmokers and in the 4-h smoking-cessation group followed by the 10-d and 21-d smoking-cessation groups. The peaks of radioactivity occurred ~50 min after injection of ^{123}I-5IA for nonsmokers and for the 4-h and 21-d smoking-cessation groups, whereas it was at ~70 min for the 10-d smoking-cessation group. A differential dissociation of ^{123}I-5IA from the binding sites was noted in the brain. The 4-h smoking-cessation group showed a faster dissociation compared with that of the nonsmokers. However, the 10-d and 21-d smoking-cessation groups showed a slower dissociation than that of the nonsmokers (more pronounced in the 21-d group). These findings reflected a temporal change of the nAChRs in the human brain.

Packs per day and pack years of cigarette smoking before cessation were similar for the different groups of smokers (Table 2). Only 2 subjects (subjects 7 and 11) had detectable amounts of nicotine in their plasma after 4-h smoking cessation (Table 2).

To validate the *Vt* values of the nonsmokers as a baseline group, we compared (*t* test) our current data (nonsmokers) with our published data (*19*). No significant difference was observed between these groups. Similar findings were also seen for K_1 and k_2. Therefore, we used the *Vt* values from nonsmokers as a reference for further comparisons with groups of smokers at several smoking-cessation intervals.

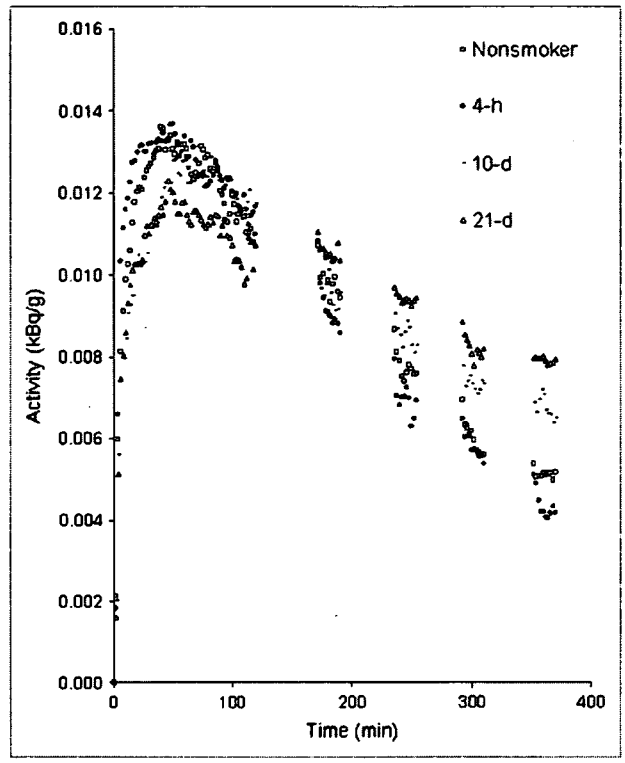

FIGURE 1. Representative standardized time–activity curves of ^{123}I-5IA in frontal cortex from a nonsmoker and smokers.

Table 3 describes the *Vt* values of different groups of volunteers (nonsmokers and smokers). There was a significant difference among those groups (ANOVA; $P < 0.001$). Individualized comparisons between 2 groups of volunteers were also performed. After 4 h of smoking cessation, the *Vt* values in all brain regions decreased significantly compared with those of the nonsmoker group ($P < 0.05$, except for frontal, parietal, and occipital cortices). On the other hand, after 10 d of smoking cessation, the *Vt* values were significantly higher than those of nonsmokers ($P < 0.05$, except for basal ganglia and thalamus). Then, after 21 d of smoking cessation, the *Vt* values decreased significantly compared

TABLE 2
Characteristics of Volunteers and Plasma Concentration of Nicotine and Cotinine

Group	Age (y ± SD)	Packs/d	Pack years	Plasma concentration (ng/mL)	
				Nicotine	Cotinine
Nonsmokers	24 ± 6	—	—	ND	ND
Smokers					
4-h withdrawal	28 ± 4	0.8 ± 0.3	6.1 ± 4.3	7.6, 8.9*	282 ± 189
10-d withdrawal	27 ± 6	0.8 ± 0.2	6.3 ± 3.9	ND	ND
21-d withdrawal	28 ± 3	0.8 ± 0.3	6.3 ± 4.5	ND	ND

*Results from only 2 subjects (3 other subjects had nondetectable values).
Packs/d = number of packs smoked per day; Pack years = number of packs per day while smoking multiplied by number of years smoked; ND = not detected (detection limits for nicotine and cotinine were 5.0 and 100 ng/mL, respectively).
Values are expressed in mean ± SD.

TABLE 3

^{123}I-5IA V_t Estimates for 2-Compartment, 2-Parameter Model for Various Brain Regions from Nonsmokers and Smokers After Withdrawal of Cigarette Smoking

Subject	Frontal	Parietal	Temporal	Occipital	BG	Thalamus	BS	Cerebellum
Nonsmokers								
1	14.3	13.2	13.2	11.2	15.8	30.1	22.9	15.6
2	20.3	18.9	19.7	16.2	24.2	43.2	35.5	20.5
3	14.1	13.0	13.8	11.2	16.0	28.4	22.3	14.9
4	14.4	14.4	14.6	11.7	17.2	31.1	25.3	18.4
5	11.3	10.7	10.7	9.5	12.9	19.3	17.7	14.4
6	13.2	12.2	12.2	11.1	13.5	20.9	18.7	13.7
Mean	14.6	13.7	14.0	11.8	16.6	28.8	23.7	16.3
SD	3.0	2.8	3.1	2.3	4.0	8.6	6.4	2.7
Smokers								
4-h withdrawal								
7	6.1	6.3	6.4	5.9	6.5	7.0	7.0	5.9
8	12.6	13.0	12.2	11.4	12.8	16.1	14.0	11.3
9	14.9	14.0	13.7	12.5	15.0	21.3	19.4	14.4
10	8.7	8.4	8.6	7.6	10.0	13.5	12.2	8.8
11	10.2	10.4	10.2	9.0	11.2	12.9	12.3	10.0
Mean	10.5	10.4	10.2	9.3	11.1	14.1	13.0	10.1
SD	3.4	3.2	2.9	2.7	3.2	5.2	4.4	3.1
10-d withdrawal								
7	19.7	19.3	19.2	17.5	21.0	31.1	29.4	20.9
8	19.1	18.7	17.4	16.4	19.4	28.7	25.3	20.7
12	18.0	17.6	17.4	16.1	20.2	28.9	30.3	22.4
13	16.1	16.2	16.4	15.2	18.7	28.9	29.3	20.8
14	19.2	18.1	17.8	15.8	21.5	36.5	32.8	23.9
Mean	18.4	18.0	17.6	16.2	20.2	30.8	29.4	21.7
SD	1.4	1.2	1.0	0.9	1.2	3.3	2.7	1.4
21-d withdrawal								
9	15.3	14.6	14.6	12.2	17.6	28.4	23.6	19.7
10	14.4	14.3	13.8	12.1	17.5	31.3	24.9	17.2
11	17.0	16.6	15.9	13.6	18.5	27.0	26.1	20.1
14	14.1	14.0	13.6	12.8	15.5	21.6	21.0	15.7
15	14.4	14.1	13.6	12.2	15.7	27.0	22.7	15.7
Mean	15.1	14.7	14.3	12.6	17.0	27.0	23.7	17.7
SD	1.2	1.1	1.0	0.6	1.3	3.5	2.0	2.1

BG = basal ganglia; BS = brain stem.
Reported as mean for V_t estimates from 2-compartment model. Values for V_t are in mL/g.

with those of the 10-d group ($P < 0.01$, except for thalamus), returning to the level in nonsmokers (Vt values did not show any significant difference compared with those in the nonsmokers). Figure 2 shows the percentage of reduction and increment in each group of smokers in comparison with the nonsmoker group. In the Tukey–Kramer multiple comparison test, the interval changes of the ^{123}I-5IA Vt between the 3 phases after the smoking cessation were significantly different ($P < 0.001$).

The rate constant K_1 had some fluctuations among the different groups of volunteers (nonsmokers and smokers); however, these differences were not statistically significant (ANOVA; not significant) (Fig. 3A). On the other hand, the values of the rate constant k_2 were significantly different among the groups of volunteers (ANOVA; $P < 0.01$) (Fig. 3B). This difference was due basically to the increase of k_2 in the group with 4 h of smoking cessation.

DISCUSSION

The present study described the effect of nicotine intake in tobacco smokers and smoking cessation on the high-affinity nicotinic receptors in humans using ^{123}I-5IA SPECT. To our knowledge, this is the first in vivo imaging of nAChR up-regulation and recovery in response to short-term smoking cessation in living smokers.

Previous animal studies have shown that chronic nicotine treatment induces an increase in high-affinity nicotinic receptor binding (*6–9*), and human postmortem studies have found a similar increase in ^{3}H-nicotine binding to high-affinity receptors in the postmortem cortex, cerebellum, and hippocampus of smokers compared with that in nonsmokers (*10–12*).

The mechanism by which the chronic exposure of nicotine evokes an increase in the density of the binding sites is not fully understood. Marks et al. reported that the increase in nicotinic receptor numbers in rodents is not caused by an

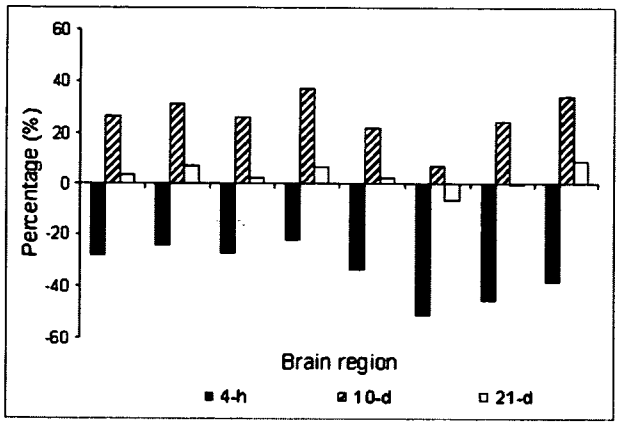

FIGURE 2. Percentage of reduction and increment of *Vt* of ^{123}I-5IA in smokers after smoking cessation compared with nonsmokers. Eight brain regions are frontal, parietal, temporal, occipital, basal ganglia, thalamus, brain stem, and cerebellum from the left, respectively.

increase in messenger RNA levels (*20*). The lack of an effect on nicotinic receptor transcription in mice suggests that nicotine-induced increases in nicotinic receptor levels are most likely related to a decrease in receptor turnover (*21*). The increase in nicotinic receptor number and the decreased rate of receptor turnover may be related to nicotinic receptor channel desensitization, which appears to reflect the conformational state of the receptor channel (*21,22*). Once the nicotinic receptor channels are desensitized and rendered inactive, additional receptors would be recruited to maintain the nicotinic response of the neuron, which results in an overall increase in nicotine binding, possibly due to a conversion of low-affinity receptors to a conformation with a high affinity for agonists (*23*).

In this study, the ^{123}I-5IA *Vt* measured at 4 h after smoking cessation was significantly lower than that in nonsmokers. The mean value of the calculated *Vt* of the smokers was ~33.5% ± 10.5% lower than that of nonsmokers and was more pronounced in the thalamus (51%) and brain stem (45%). In this group of volunteers, the plasma nicotine level 4 h after smoking cessation was detectable in only 2 subjects and was below the detection limit in the other subjects. Nicotine is highly lipophilic and demonstrated high levels of nonspecific uptake in brain (*24,25*). Rowell and Li have reported that levels of nicotine in the brain were ~3-fold higher than those in the plasma (*7*), which explains the lack of plasma nicotine measurements in 3 subjects in this group of volunteers. Because of high levels of nonspecific uptake of nicotine in the brain, nicotine or its metabolites may accumulate in nonspecific compartments in the brain (i.e., white matter) and then diffuse slowly into areas with higher levels of nAChRs, maintaining high levels of occupancy of the nAChRs. In addition, Brody et al. have shown saturation of the nicotinic receptors in human brain for up to 4 h in smokers (*26*). Thus, we would expect some level of nicotine or metabolites in the brain that would compete with ^{123}I-5IA and impair imaging of the upregulation of nAChRs. Also, we believe that some level of nicotine in the brain resulted in a high level of occupancy of the receptors, which reduced specific tracer uptake (*27*). Because of competitive binding between the radioligand and nicotine in the brain, imaging of upregulation of nAChRs in vivo requires sufficient time for nicotine clearance (>4-h smoking cessation).

After 10 d of smoking cessation, the *Vt* of ^{123}I-5IA was significantly higher than that in nonsmokers, with a 25.7% ± 9.2% increase among brain regions. The result of the increased *Vt* of the ^{123}I-5IA was in agreement with the upregulation of the nAChRs in the brains of smokers reported in postmortem human studies (*10–12*) and in animal studies (*6–9*). Staley et al. have described similar findings in human brain (*13*). The authors noted that after 6.8 ± 1.9 d of tobacco abstinence, the uptake of ^{123}I-5IA increased significantly throughout the cerebral cortex (26%~36%) in smokers (*13*). After 10 d of smoking cessation, nicotine and cotinine were not detected in the plasma. Thus, blood nicotine levels were negligible in the ^{123}I-5IA SPECT scans of smokers as well as nonsmokers.

After 21 d of smoking cessation, the *Vt* of ^{123}I-5IA was significantly lower compared with that after 10 d of smoking cessation and was not significantly different from that in the nonsmokers. Breese et al. showed that smokers who had quit at least 2 mo before death had nicotinic receptor binding levels similar to those in nonsmokers (*14*). In the present study, the interval of 21 d was thought to be the recovery time during which upregulated nAChRs return to the level of the nonsmoker. This suggests that nicotine-induced upregulation of receptor number is a temporary effect, similar to that found in rodents (*28,29*).

The upregulation of the nAChRs was similar in almost all brain regions, except the thalamus and basal ganglia, which showed a slightly different pattern. In thalamus and basal ganglia, after 10 d of smoking cessation the *Vt* was higher than that of the nonsmokers, as in the other regions, but was not significantly different. Staley et al. have shown similar findings (*13*). In addition, it has been reported in a study of mice that nicotine-induced increases in nicotinic receptor numbers do not increase to the same degree in all brain regions (*30*). Moreover, the nicotinic receptor is more abundant in the thalamus, with greater receptor heterogeneity, than in other brain regions (*19*). However, the characteristics of the acute response of neuronal nAChRs to nicotine depend on their subunit composition (*31,32*). Nicotinic receptor subtypes are affected differentially by chronic exposure to nicotine, both in cell models (*33–35*) and in vivo (*35*). Multiple factors are thought to be responsible for these differences.

This study should be interpreted in the context of several limitations. (a) The number of subjects evaluated was small, which reduced the statistical accuracy. (b) The study design used did not allow us to deal with a within-subject analysis of the whole group, as the variables were analyzed independently. (c) The smokers varied in their rate and depth of inhalation of smoke, and these interindividual

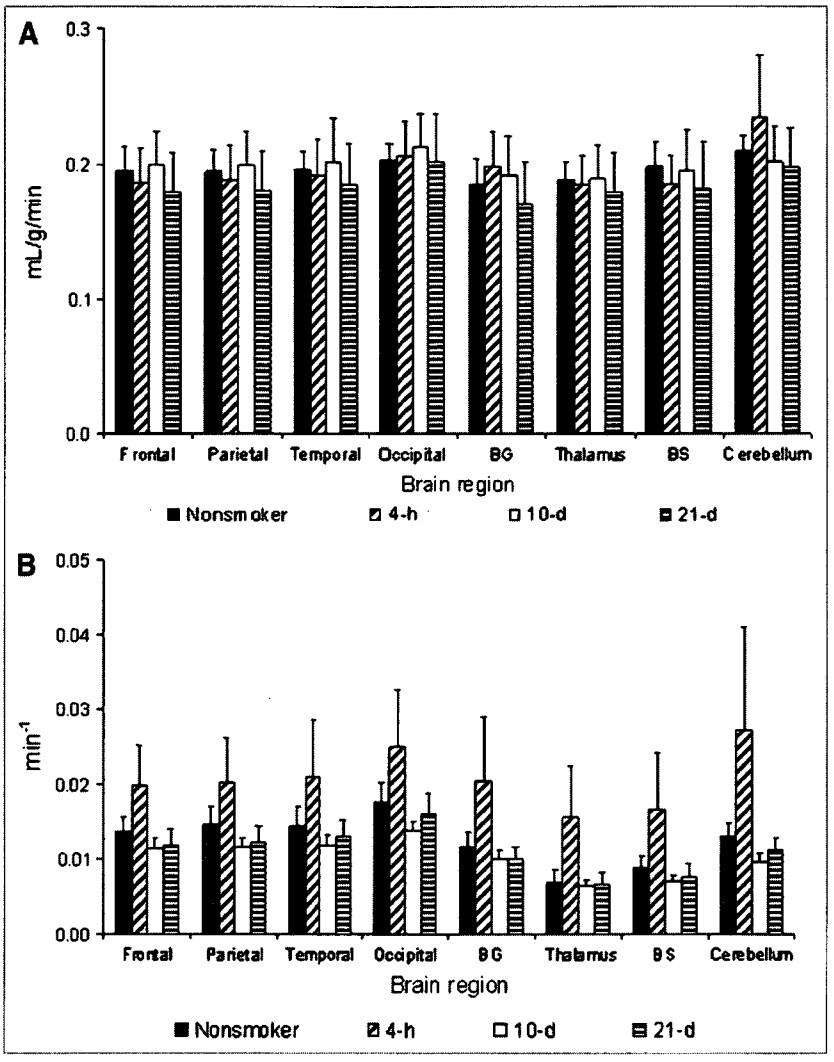

FIGURE 3. Temporal changes in rate constants K_1 and k_2 in nonsmokers and smokers after smoking cessation. (A) Rate constant K_1 (mL/g/min). (B) Rate constant k_2 (min^{-1}). BG = basal ganglia; BS = brain stem.

differences could have affected our measurements. (d) The detection limit of the plasma nicotine measurements was not enough to evaluate all blood samples. Thus, we were not able to correlate the plasma nicotine/cotinine levels with *Vt*. (e) We have not coregistered SPECT images with MRI, which would have been the most appropriate method for placement of ROIs. (f) We have not evaluated the smoker's behavior during the smoking-cessation period. We believe that the nicotine binding and desensitization of the nAChRs in the brain alleviate the cigarette craving and that craving will be the worst during the first 10 d of cessation due to the upregulation of nAChRs. The craving process should minimize after 21 d, as we observe similar levels of occupancy as nonsmokers at that time. However, we cannot exclude the possibility of other nAChR subtypes being involved in the process of tobacco dependence.

CONCLUSION

We have described the in vivo imaging of nAChR upregulation and recovery in response to short-term smoking cessation in smokers using ^{123}I-5IA SPECT. Our results clearly suggest that tobacco smoking is associated with an upregulation of nicotine binding sites in the brain. The upregulation of the nAChRs of the smokers after chronic exposure to nicotine was downregulated to the level in nonsmokers after ~21 d of smoking cessation. Thus, the upregulation of receptor numbers is a temporary effect. Nicotine dependence and difficulty in smoking cessation are also interesting with regard to the findings of the ^{123}I-5IA SPECT study. The decrease in nicotinic receptors to nonsmoker levels may be the breaking point during the nicotine withdrawal period.

ACKNOWLEDGMENTS

The authors thank Dr. Masanori Ichise (Department of Radiology, Columbia University, College of Physicians and Surgeons) for his tremendous editorial support and suggestions on this project. The authors also thank Nihon Medi-Physics Co. Ltd., Japan, for providing sodium ^{123}I-iodide.

This work was supported in part by a grant from the Research for the Future Program of the Japan Society for the Promotion of Science (JSPS-RFTF97K00201); Grants-in-Aid for Scientific Research from the Ministry of Education, Science and Technology of Japan; a research grant from Longevity Sciences from the Ministry of Health and Welfare; and a grant from the Smoking Research Foundation.

REFERENCES

1. Gotti C, Fornasari D, Clementi F. Human neuronal nicotinic receptors. *Prog Neurobiol.* 1997;53:199–237.
2. Paterson D, Nordberg A. Neuronal nicotinic receptors in the human brain. *Proc Neurobiol.* 2000;61:75–111.
3. Shimohama S, Kihara T. Nicotinic receptor-mediated protection against beta-amyloid neurotoxicity. *Biol Psychiatry.* 2001;49:233–239.
4. Decker MW, Rueter LE, Bitner RS. Nicotinic acetylcholine receptor agonists: a potential new class of analgesics. *Curr Top Med Chem.* 2004;4:369–384.
5. Buisson B, Bertrand D. Nicotine addiction: the possible role of functional up-regulation. *Trends Pharmacol Sci.* 2002;23:130–136.
6. Pietila K, Lahde T, Attila M, Ahtee L, Nordberg A. Regulation of nicotinic receptors in the brain of mice withdrawn from chronic oral nicotine treatment. *Naunyn Schmiedebergs Arch Pharmacol.* 1998;357:176–182.
7. Rowell PP, Li M. Dose-response relationship for nicotine-induced up-regulation of rat brain nicotinic receptors. *J Neurochem.* 1997;68:1982–1989.
8. Collins AC, Romm E, Wehner JM. Dissociation of the apparent relationship between nicotine tolerance and up-regulation of nicotinic receptors. *Brain Res Bull.* 1990;25:373–379.
9. Koylu E, Demirgoren S, London ED, Pogun S. Sex difference in up-regulation of nicotinic acetylcholine receptors in rat brain. *Life Sci.* 1997;61:L185–L190.
10. Perry DC, Davila-Garcia MI, Stockmeier CA, Kellar KJ. Increased nicotinic receptors in brains from smokers: membrane binding and autoradiography studies. *J Pharmacol Exp Ther.* 1999;289:1545–1552.
11. Teaktong T, Graham AJ, Johnson M, Court JA, Perry EK. Selective changes in nicotinic acetylcholine receptor subtypes related to tobacco smoking: an immunohistochemical study. *Neuropathol Appl Neurobiol.* 2004;30:243–254.
12. Kassiou M, Eberl S, Meikle SR, et al. In vivo imaging of nicotinic receptor upregulation following chronic (-)-nicotine treatment in baboon using SPECT. *Nucl Med Biol.* 2001;28:165–175.
13. Staley JK, Krishnan-Sarin S, Cosgrove KP, et al. Human tobacco smokers in early abstinence have higher of b2* nicotinic acetylcholine receptors than non-smokers. *J Neurosci.* 2006;26:8707–8714.
14. Breese CR, Marks MJ, Logel MJ, et al. Effect of smoking history on [^{3}H]nicotine binding in human postmortem brain. *J Pharmacol Exp Ther.* 1997; 282:7–13.
15. Saji H, Ogawa M, Ueda M, et al. Evaluation of radioiodinated 5-iodo-3-(2(S)-azetidinylmethoxy)pyridine as a ligand for SPECT investigations of brain nicotinic acetylcholine receptors. *Ann Nucl Med.* 2002;16:189–200.
16. Musachio JL, Scheffel U, Finley PA, et al. 5-[I-125/123]Iodo-3(2(S)-azetidinylmethoxy)pyridine, a radioiodinated analog of A-85380 for in vivo studies of central nicotinic acetylcholine receptors. *Life Sci.* 1998;62:351–357.
17. Ueda M, Iida Y, Mukai T, et al. 5-[^{123}I]Iodo-A-85380: assessment of pharmacological safety, radiation dosimetry and SPECT imaging of brain nicotinic receptors in healthy human subjects. *Ann Nucl Med.* 2004;18: 337–344.
18. Vaupel DB, Tella SR, Huso DL, et al. Pharmacology, toxicology, and radiation dosimetry evaluation of [I-123]5-I-a-85380, a radioligand for in vivo imaging of cerebral neuronal nicotinic acetylcholine receptors in humans. *Drug Dev Res.* 2003;58:149–168.
19. Mamede M, Ishizu K, Ueda M, et al. Quantification of human nicotinic acetylcholine receptors with ^{123}I-5IA SPECT. *J Nucl Med.* 2004;45:1458–1470.
20. Marks MJ, Pauly JR, Gross SD, et al. Nicotine binding and nicotinic receptor subunit RNA after chronic nicotine treatment. *J Neurosci.* 1992;12:2765–2784.
21. Peng X, Gerzanich V, Anand R, Whiting PJ, Lindstrom J. Nicotine-induced increase in neuronal nicotinic receptors results from a decrease in the rate of receptor turnover. *Mol Pharmacol.* 1994;46:523–530.
22. Marks MJ, Burch JB, Collins AC. Genetics of nicotine response in four inbred strains of mice. *J Pharmacol Exp Ther.* 1983;226:291–302.
23. Bencherif M, Fowler K, Lukas RJ, Lippiello PM. Mechanisms of up-regulation of neuronal nicotinic acetylcholine receptors in clonal cell lines and primary cultures of fetal rat brain. *J Pharmacol Exp Ther.* 1995;275:987–994.
24. Broussolle EP, Wong DF, Fanelli FJ, London ED. In vivo specific binding of [^{3}H]l-nicotine in the mouse brain. *Life Sci.* 1989;44:1123–1132.
25. Muzic R, Berridge M, Friedland R, Zhu N, Nelson A. PET quantification of specific binding of carbon-11-nicotine in human brain. *J Nucl Med.* 1998;39: 2048–2054.
26. Brody AL, Mandelkern MA, London ED, et al. Cigarette smoking saturates brain α4β2 nicotinic acetylcholine receptors. *Arch Gen Psychiatry.* 2006;63: 907–915.
27. Ding Y-S, Volkow ND, Logan J, et al. Occupancy of brain nicotinic acetylcholine receptors by nicotine doses equivalent to those obtained when smoking a cigarette. *Synapse.* 2000;35:234–237.
28. Collins AC, Bhat RV, Pauly JR, Marks MJ. Modulation of nicotine receptors by chronic exposure to nicotinic agonists and antagonists. *Ciba Found Symp.* 1990; 152:68–82.
29. Marks MJ, Stitzel JA, Collins AC. Time course study of the effects of chronic nicotine infusion on drug response and brain receptors. *J Pharmacol Exp Ther.* 1985;235:619–628.
30. Collins AC, Marks MJ, Pauly JR. Differential effect of chronic nicotine treatment on nicotinic receptor numbers in various brain regions of mice. *J Subst Abuse.* 1989;1:273–286.
31. Luetje CW, Patrick J. Both α and β subunits contribute to the agonist sensitivity of neuronal acetylcholine receptors. *J Neurosci.* 1991;11:837–845.
32. Fenster CP, Rains MF, Noerager B, Quick MW, Lester RAJ. Influence of subunit composition on desensitization of neuronal acetylcholine receptors at low concentrations of nicotine. *J Neurosci.* 1997;17:5747–5759.
33. Hsu Y-N, Amin J, Weiss DS, Wecker L. Sustained nicotine exposure differentially affects α3β2 and α4β2 neuronal nicotinic receptors expressed in *Xenopus* oocytes. *J Neurochem.* 1996;66:667–675.
34. Olale F, Gerznich V, Kurytov A, Wang F, Lindstrom J. Chronic nicotine exposure differentially affects the function of human α3, α4 and α7 neuronal nicotinic receptor subtypes. *J Pharmacol Exp Ther.* 1997;283:675–683.
35. Peng X, Gerzanich V, Anand R, Wang F, Lindstrom J. Chronic nicotine treatment up-regulates α3 and α7 acetylcholine receptor subtypes expressed by the human neuroblastoma cell line SH-SY5Y. *Mol Pharmacol.* 1997;51:776–784.

Eur Radiol (2007) 17: 2921–2925
DOI 10.1007/s00330-007-0688-9

NEURO

Yasutaka Fushimi
Yukio Miki
Shin-ichi Urayama
Tsutomu Okada
Nobuyuki Mori
Takashi Hanakawa
Hidenao Fukuyama
Kaori Togashi

Gray matter-white matter contrast on spin-echo T1-weighted images at 3 T and 1.5 T: a quantitative comparison study

Received: 8 August 2006
Revised: 31 January 2007
Accepted: 8 May 2007
Published online: 7 July 2007
© Springer-Verlag 2007

This study was supported in part by a Health and Labour Sciences Research Grant of Japan.

Yasutaka Fushimi and Yukio Miki equally contributed to the study.

Y. Fushimi · Y. Miki (✉) · T. Okada · N. Mori · K. Togashi
Department of Diagnostic Imaging and Nuclear Medicine, Kyoto University Graduate School of Medicine,
54 Shogoin-Kawaharacho, Sakyo-ku,
Kyoto, 606-8507, Japan
e-mail: mikiy@kuhp.kyoto-u.ac.jp
Tel.: +81-75-7513710
Fax: +81-75-7719709

S.-i. Urayama · T. Hanakawa · H. Fukuyama
Human Brain Research Center,
Kyoto University Graduate School of Medicine,
Kyoto, Japan

T. Hanakawa
Department of Cortical Function Disorders, National Institute of Neuroscience, National Center of Neurology and Psychiatry,
Kyoto, Japan

Abstract Discrepancies exist in the literature regarding contrast between gray and white matter on spin-echo (SE) T1-weighted MR imaging at 3 T. The present study quantitatively assessed differences in gray matter-white matter contrast on both single- and multi-slice SE T1-weighted imaging between 3 and 1.5 T. SE T1-weighted sequences with the same parameters at both 3 and 1.5 T were used. Contrast-to-noise ratio (CNR) between gray and white matter ($CNR_{GM\text{-}WM}$) was evaluated for both frontal lobes. To assess the effects of interslice gap, multi-slice images were obtained with both 0 and 25% interslice gap. Single-slice $CNR_{GM\text{-}WM}$ was higher at 3 T (17.66±2.68) than at 1.5 T (13.09±2.35; $P<0.001$). No significant difference in $CNR_{GM\text{-}WM}$ of multi-slice images with 0% gap was noted between 3 and 1.5 T (3T, 8.61±2.55; 1.5T, 7.43±1.20; $P>0.05$). Multi-slice $CNR_{GM\text{-}WM}$ with 25% gap was higher at 3T (12.47±3.31) than at 1.5 T (9.73±1.37; $P<0.001$). $CNR_{GM\text{-}WM}$ reduction rate of multi-slice images with 0% gap compared with single-slice images was higher at 3T (0.47±0.13) than at 1.5 T (0.38±0.09; $P=0.02$). $CNR_{GM\text{-}WM}$ on single-slice SE T1-weighted imaging and $CNR_{GM\text{-}WM}$ on multi-slice images with 25% interslice gap were better at 3 T than at 1.5 T. The influence of multi-slice imaging on $CNR_{GM\text{-}WM}$ was significantly larger at 3T than at 1.5 T.

Keywords High-field MR · Brain · Magnetic resonance imaging · T1-weighted image

Introduction

Magnetic resonance (MR) imaging at 3 T has gradually been introduced to clinical practice in addition to research fields. Signal-to-noise ratio (SNR) is better at 3 T MR imaging than at 1.5 T MR imaging [1–4]. This improved SNR at 3 T MR imaging provides advantages in various applications [5–7]. Increased T1 relaxation time and improved SNR at 3 T provide better visualization on MR angiography [8, 9].

Discrepancies exist in the literature regarding contrast between gray matter (GM) and white matter (WM) on spin-echo (SE) T1-weighted MR imaging at 3 T. Nobauer-Huhmann et al. [10] reported that visual assessment of

differentiation between GM and WM on SE T1-weighted sequences was significantly lower at 3 T than at 1.5 T. They noted that the repetition time (TR) optimized for 1.5 T was too long to obtain sufficient contrast between GM and WM at 3 T. A review by Scarabino et al. [11] stated that SE T1-weighted images show low contrast-to-noise ratio (CNR) between GM and WM (CNR_{GM-WM}), probably due to longer T1 relaxation time at 3T. Sasaki et al. [12] commented that delayed magnetization recovery due to longer T1 relaxation time reduces contrast between GM and WM on SE T1-weighted imaging at 3 T. Ross [13] indicated in an editorial that quality of SE T1-weighted imaging is degraded by longer T1 relaxation time and chemical shift. Conversely, Lu et al. [14] recently published data showing CNR_{GM-WM} increased by 20.7% on SE T1-weighted imaging at 3T compared with CNR_{GM-WM} at 1.5 T by optimizing imaging parameters for each magnet. In addition, Schmitz et al. [15] demonstrated that SE T1-weighted imaging could display better CNR at 3 T by adjusting flip angles.

To the best of our knowledge, no comparison studies featuring CNR_{GM-WM} of SE T1-weighted sequences with the same imaging parameters at 3 and 1.5 T have been reported. Differences in CNR_{GM-WM} between single- and multi-slice SE T1-weighted sequences have also not been well studied for 3 and 1.5 T.

The present study quantitatively examined differences in CNR_{GM-WM} for both single- and multi-slice SE T1-weighted images using the same imaging parameters between 3 and 1.5 T.

Materials and methods

Subjects

Subjects comprised 10 healthy volunteers (7 males, 3 females, range 25–36 years, average 29 years). All subjects were neurologically examined by a neurologist (T.H.) and were considered neurologically healthy. The local ethical committee approved the study protocols, and all subjects provided written informed consent before entering the study.

Imaging protocols

All subjects underwent both 3 and 1.5 T imaging on the same day in random order, using a 3 T MR scanner (Magnetom Trio, Siemens, Erlangen, Germany) and a 1.5 T MR scanner (Magnetom Symphony, Siemens, Erlangen, Germany). The interval between imagings was <30 min. The body coil was not standard equipment at 3 T; therefore, the head coil was used as a transmission coil. The standard setup of body coil transmission was used at 1.5 T. The image center was shared between both MR units by posting markers on the face of each subject. A circular polarized head coil was used, and the head was firmly fixed using foam pads. Subjects were instructed not to move during MR imaging. Imaging slices were positioned parallel to the anterior commissure-posterior commissure line at the level of the basal ganglia.

Imaging parameters

SE T1-weighted sequence that was routinely used at 1.5 T was applied for both 3 and 1.5 T imaging: TR 600 ms; echo time (TE) 20 ms; slice thickness 5 mm; number of averages 1; matrix 256×256; flip angle 90°; bandwidth 90 Hz; scan time 2 min 38 s. Within each subject, this sequence was repeated with the image center fixed for the single slice, multi-slice with 0% gap (gapless), and multi-slice with 25% interslice gap (1.25-mm interslice gap) (Fig. 1). The number of multi-slice images was set as seven due to high systemic absorption rate (SAR) at 3 T.

Analysis of regions of interest

GM and WM of frontal lobes and background were selected as regions of interest (ROI) on the center slice of each SE T1-weighted image (Fig. 2). In each subject, the same ROIs were applied for all images. CNR_{GM-WM} was defined as the difference between intensities of GM and WM divided by the standard deviation of the background [16]. ROIs were drawn using ImageJ software (National Institutes of Health, Bethesda, MD, USA).

Statistical analysis

Two-sided paired *t*-test was applied using JMP 5.1 (SAS Institute, Cary, NC, USA). Values of $P<0.05$ were considered statistically different.

Results

Single-slice CNR_{GM-WM} was significantly higher at 3 T (17.66±2.68) than at 1.5 T (13.09±2.35) ($P<0.001$) (Fig. 3). A 1.37±0.23-fold gain in CNR_{GM-WM} was seen for single slice at 3 T compared with 1.5 T.

No significant difference in multi-slice CNR_{GM-WM} was noted with 0% gap (3 T: 8.61±2.55; 1.5T: 7.43±1.20; $P>0.05$) between 3 and 1.5 T. Multi-slice CNR_{GM-WM} with 25% gap was higher at 3 T (12.47±3.31) than at 1.5 T (9.73±1.37; $P<0.001$) (Fig. 3).

CNR_{GM-WM} reduction rate for multi-slice with 0% gap from single-slice was higher at 3 T (0.47±0.13) than at

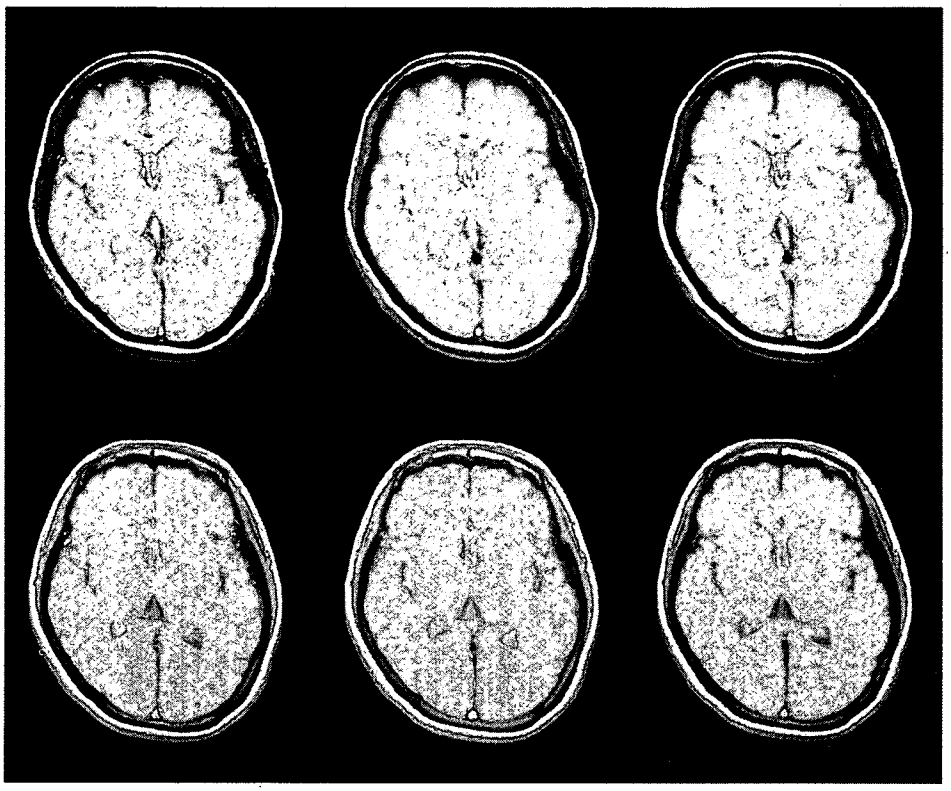

Fig. 1 SE T1-weighted imaging at 3 T (*upper row*) and 1.5 T (*lower row*). From *left* to *right*, total imaging slices are 1 (single slice), multi-slices with 0% interslice gap, and multi-slices with 25% interslice gap. Contrast between GM and WM at 3 and 1.5 T is more conspicuous in a single slice than in multi-slices. Contrast between GM and WM of a single slice is obviously better at 3 T than at 1.5 T. Contrast between GM and WM for multi-slices with 25% interslice gap is better at 3 T than at 1.5 T

1.5 T (0.38±0.09; P=0.02) (Fig. 4). No significant difference in $CNR_{GM\text{-}WM}$ reduction rate was seen for multi-slice with 25% gap from single slice (3 T: 0.29±0.16; 1.5 T: 0.28±0.10; P>0.05) between 3 and 1.5 T (Fig. 4).

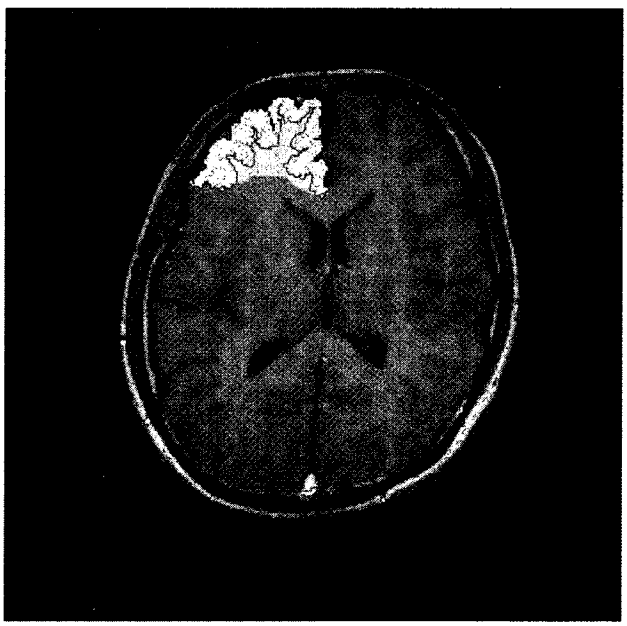

Fig. 2 A representative image of ROI on SE T1-weighted image. GM and WM of frontal lobes were selected as ROI

Discussion

Single-slice SE T1-weighted imaging produced better $CNR_{GM\text{-}WM}$ at 3 T than at 1.5 T in this study. Under the same imaging parameters for both magnetic fields, $CNR_{GM\text{-}WM}$ increased 1.37±0.23-fold at 3 T compared to 1.5 T. Lu et al. [14] reported a 20.7% increase in $CNR_{GM\text{-}WM}$ on SE T1-weighted imaging at 3 T compared with 1.5 T in five volunteers; however, imaging parameters for SE T1-weighted imaging were optimized for each magnet in their study. In this study, the same imaging parameters were applied for SE T1-weighted imaging at both 3 and 1.5 T, and better $CNR_{GM\text{-}WM}$ was seen at 3 T compared with 1.5 T. To the best of our knowledge, this is the first comparison study featuring differences in $CNR_{GM\text{-}WM}$ on SE T1-weighted imaging using the same imaging parameters at 3 and 1.5 T.

$CNR_{GM\text{-}WM}$ was decreased in multi-slice imaging with 0% gap for both magnetic fields when compared to single-slice imaging, and a larger $CNR_{GM\text{-}WM}$ reduction rate for multi-slices with 0% gap from single slice was observed at 3 T than at 1.5 T. This might be due to cross-talk effect and/or magnetization transfer (MT) effect, both of which may reduce CNR with multi-slice imaging [17]. MT effect is reportedly higher at 3 T than at 1.5 T [18, 19], partially supporting our results.

In this study, both multi-slice and gapless imaging exacerbated $CNR_{GM\text{-}WM}$ on SE T1-weighted sequences, and the degree of $CNR_{GM\text{-}WM}$ reduction was larger at 3T

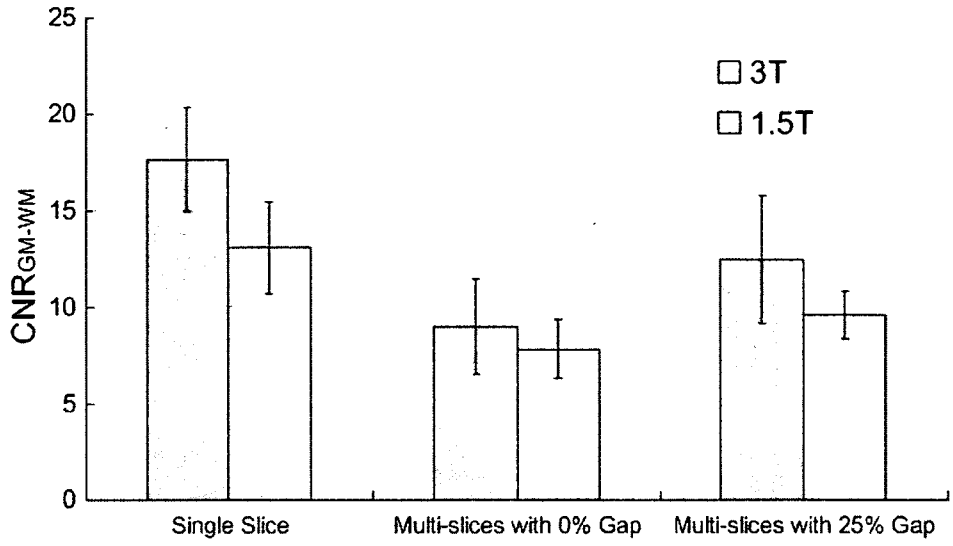

Fig. 3 $CNR_{GM\text{-}WM}$ for single slice, multi-slice with 0% gap, and multi-slice with 25% gap at 3 T (*dark gray bar*) and 1.5 T (*light gray bar*). *Error bars* represent standard deviation. Single-slice $CNR_{GM\text{-}WM}$ was higher at 3 T (17.66±2.68) than at 1.5 T (13.09±2.35; $P<0.001$). Multi-slice $CNR_{GM\text{-}WM}$ with 25% gap was higher at 3T (12.47±3.31) than at 1.5 T (9.73±1.37; $P<0.001$). No significant difference in multi-slice $CNR_{GM\text{-}WM}$ with 0% gap was noted between 3 T and 1.5 T (3T: 8.61±2.55; 1.5 T: 7.43±1.20; $P>0.05$)

than at 1.5 T. Attention must therefore be paid to the interslice gap in applying SE T1-weighted sequences at 3 T. The best $CNR_{GM\text{-}WM}$ at 3 T was obtained using single-slice imaging in this study, which of course will not likely be applicable in routine practice. However, radiologists need to know that $CNR_{GM\text{-}WM}$ on SE T1-weighted sequences is better at 3 T than at 1.5 T without the influences of multi-slice imaging. 3D gradient sequences such as magnetization prepared rapid acquisition with gradient echo (MPRAGE) or fast spoiled gradient echo (FSPGR) sequences are often used as substitutes for SE T1-weighted sequences at 3 T [10, 12], but SE T1-weighted imaging may be applicable at 3 T if sufficient interslice gap is applied and if the SAR issue is addressed.

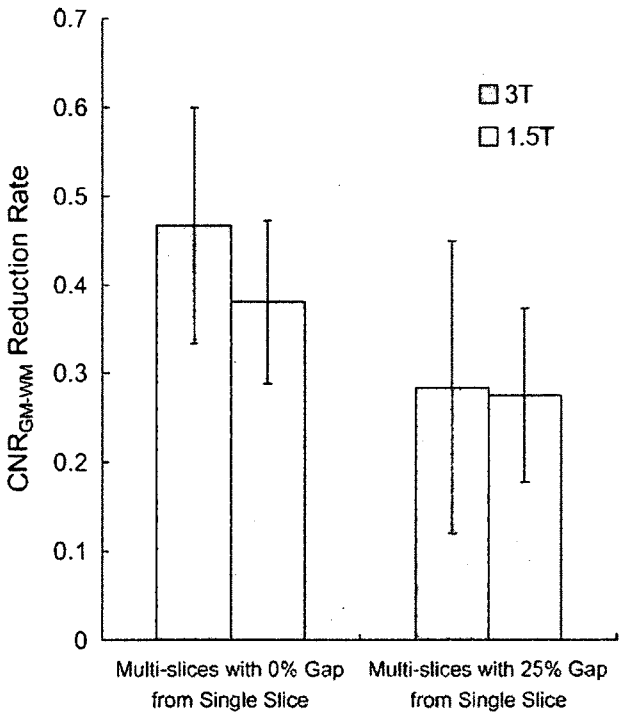

Fig. 4 $CNR_{GM\text{-}WM}$ reduction rate for multi-slice imaging with 0% gap from single-slice imaging at 3 T (*dark gray bar*) and 1.5 T (*light gray bar*). *Error bars* represent standard deviation. $CNR_{GM\text{-}WM}$ reduction rate is significantly larger at 3 T (0.47±0.13) than at 1.5 T (0.38±0.09; $P=0.02$). $CNR_{GM\text{-}WM}$ reduction rates for multi-slices with 25% gap from single-slice imaging at 3 T (*dark gray bar*) and 1.5 T (*light gray bar*) are shown. No significant difference in $CNR_{GM\text{-}WM}$ reduction rate is noted (3 T: 0.29±0.16; 1.5 T: 0.28±0.10; $P>0.05$

Relatively lower contrast between GM and WM at 3 T has been reported by various authors [10–13], but these reports have mainly been based on visual assessment. In the present study, differences in $CNR_{GM\text{-}WM}$ on SE T1-weighted imaging between 1.5 and 3 T were quantitatively evaluated for the first time. Since the intensity of the center part of images on SE T1-weighted sequences at 3 T is higher than the peripheral parts, probably due to B1 homogeneity [20, 21], display window-width could be set wider so that the center of images will not be whited-out, an effect which might prevent radiologists from noticing the true contrast between GM and WM at 3 T. Schmitz et al. [15] revealed that SE T1-weighted imaging with lower flip angles contributes to better CNR at 3 T probably because of more uniform signal intensity distribution. They achieved SE T1-weighted imaging with lower SAR at 3 T by decreasing flip angles. They also commented that there might be other factors that decrease CNR, such as magnetization transfer or shielding effects [15]. Lu et al. [14] reported that TR had more influence on $CNR_{GM\text{-}WM}$ of SE T1-weighted images at 3 T than TE. They optimized SE T1-weighted images at 3 T by plotting CNR of T1-weighted images with various TR and TE, which showed better $CNR_{GM\text{-}WM}$ than that at 1.5 T [14].

The present study displays some limitations. Identical imaging parameters were applied for 3 T SE T1-weighted sequence as for 1.5 T, which is routinely used in clinical

practice, a whole brain was not covered, and total imaging slices were limited to conform to SAR limitations at 3 T. Future studies need to optimize SE T1-weighted sequences at 3 T to obtain more imaging slices with suitable $CNR_{GM\text{-}WM}$, so that SE T1-weighted sequences can be routinely used at 3 T. According to the results of the present study, a two package of interleaved SE T1-weighted imaging with 100% interslice gap that will cover the whole brain might show better $CNR_{GM\text{-}WM}$ at 3 T. In clinical practices, SE T1-weighted imaging with reduced interslice gaps or with lower flip angles might show better $CNR_{GM\text{-}WM}$ at 3 T, however, further investigation should be done in future studies.

One possible reason for the differences in $CNR_{GM\text{-}WM}$ on SE T1-weighted imaging between 1.5 and 3 T is that a body coil was used for transmitting at 1.5 T, whereas at 3 T a head coil was used, which is known to have poorer transmission efficiency and B1 homogeneity than a body coil.

In conclusion, $CNR_{GM\text{-}WM}$ on single-slice SE T1-weighted imaging and $CNR_{GM\text{-}WM}$ on multi-slice imaging with 25% interslice gap are better at 3 T than at 1.5 T. The influence of multi-slice imaging on $CNR_{GM\text{-}WM}$ is significantly larger at 3 T than at 1.5 T.

References

1. Hoenig K, Kuhl CK, Scheef L (2005) Functional 3.0-T MR assessment of higher cognitive function: are there advantages over 1.5-T imaging? Radiology 234:860–868
2. Manka C, Traber F, Gieseke J, Schild HH, Kuhl CK (2005) Three-dimensional dynamic susceptibility-weighted perfusion MR imaging at 3.0 T: feasibility and contrast agent dose. Radiology 234:869–877
3. Frayne R, Goodyear BG, Dickhoff P, Lauzon ML, Sevick RJ (2003) Magnetic resonance imaging at 3.0 Tesla: challenges and advantages in clinical neurological imaging. Invest Radiol 38:385–402
4. Schick F (2005) Whole-body MRI at high field: technical limits and clinical potential. Eur Radiol 15:946–959
5. Moser E, Trattnig S (2003) 3.0 Tesla MR systems. Invest Radiol 38:375–376
6. Kuhl CK, Textor J, Gieseke J, von Falkenhausen M, Gernert S, Urbach H, Schild HH (2005) Acute and subacute ischemic stroke at high-field-strength (3.0-T) diffusion-weighted MR imaging: intraindividual comparative study. Radiology 234:509–516
7. Okada T, Miki Y, Fushimi Y, Hanakawa T, Kanagaki M, Yamamoto A, Urayama S, Fukuyama H, Hiraoka M, Togashi K (2006) Diffusion-tensor fiber tractography: intraindividual comparison of 3.0-T and 1.5-T MR imaging. Radiology 238:668–678
8. Bernstein MA, Huston J 3rd, Lin C, Gibbs GF, Felmlee JP (2001) High-resolution intracranial and cervical MRA at 3.0T: technical considerations and initial experience. Magn Reson Med 46:955–962
9. Fushimi Y, Miki Y, Kikuta K, Okada T, Kanagaki M, Yamamoto A, Nozaki K, Hashimoto N, Hanakawa T, Fukuyama H, Togashi K (2006) Comparison of 3.0- and 1.5-T three-dimensional time-of-flight MR angiography in Moyamoya disease: preliminary experience. Radiology 239:232–237
10. Nobauer-Huhmann IM, Ba-Ssalamah A, Mlynarik V, Barth M, Schoggl A, Heimberger K, Matula C, Fog A, Kaider A, Trattnig S (2002) Magnetic resonance imaging contrast enhancement of brain tumors at 3 tesla versus 1.5 tesla. Invest Radiol 37:114–119
11. Scarabino T, Nemore F, Giannatempo GM, Bertolino A, Di Salle F, Salvolini U (2003) 3.0 T magnetic resonance in neuroradiology. Eur J Radiol 48:154–164
12. Sasaki M, Inoue T, Tohyama K, Oikawa H, Ehara S, Ogawa A (2003) High-field MRI of the central nervous system: current approaches to clinical and microscopic imaging. Magn Reson Med Sci 2:133–139
13. Ross JS (2004) The high-field-strength curmudgeon. AJNR Am J Neuroradiol 25:168–169
14. Lu H, Nagae-Poetscher LM, Golay X, Lin D, Pomper M, van Zijl PC (2005) Routine clinical brain MRI sequences for use at 3.0 Tesla. J Magn Reson Imaging 22:13–22
15. Schmitz BL, Gron G, Brausewetter F, Hoffmann MH, Aschoff AJ (2005) Enhancing gray-to-white matter contrast in 3 T T1 spin-echo brain scans by optimizing flip angle. AJNR Am J Neuroradiol 26:2000–2004
16. Constable RT, Henkelman RM (1991) Contrast, resolution, and detectability in MR imaging. J Comput Assist Tomogr 15:297–303
17. Majumdar S, Sostman HD, MacFall JR (1989) Contrast and accuracy of relaxation time measurements in acquired and synthesized multislice magnetic resonance images. Invest Radiol 24:119–127
18. Schmitz BL, Aschoff AJ, Hoffmann MH, Gron G (2005) Advantages and pitfalls in 3T MR brain imaging: a pictorial review. AJNR Am J Neuroradiol 26:2229–2237
19. Stanisz GJ, Odrobina EE, Pun J, Escaravage M, Graham SJ, Bronskill MJ, Henkelman RM (2005) T1, T2 relaxation and magnetization transfer in tissue at 3T. Magn Reson Med 54:507–512
20. Vaughan JT, Garwood M, Collins CM, Liu W, DelaBarre L, Adriany G, Andersen P, Merkle H, Goebel R, Smith MB, Ugurbil K (2001) 7 T vs. 4 T: RF power, homogeneity, and signal-to-noise comparison in head images. Magn Reson Med 46:24–30
21. Collins CM, Liu W, Schreiber W, Yang QX, Smith MB (2005) Central brightening due to constructive interference with, without, and despite dielectric resonance. J Magn Reson Imaging 21:192–196